Molecular-beam resonance method with Zeeman-decelerated samples: Application to metastable helium molecules

Author(s):
Semeria, Luca; Jansen, Paul; Clausen, Gloria; Agner, Josef A.; Schmutz, Hansjürg; Merkt, Frédéric

Publication date:
2018-12

Permanent link:
https://doi.org/10.3929/ethz-b-000313508

Originally published in:
Physical Review A 98(6), https://doi.org/10.1103/physreva.98.062518

Funding acknowledgement:
743121 - Cold Ion Chemistry - Experiments within a Rydberg Orbit (EC)

The following article appeared in *Phys. Rev. A* **98**, 062518 (2018) and may be found at https://doi.org/10.1103/PhysRevA.98.062518.

Molecular-beam resonance method with Zeeman-decelerated samples: Application to metastable helium molecules

Luca Semeria, Paul Jansen, Gloria Clausen, Josef A. Agner, Hansjürg Schmutz, and Frédéric Merkt*
Laboratory of Physical Chemistry, ETH Zurich, CH-8093 Zurich, Switzerland

(Received 17 July 2018; published 26 December 2018)

We use a multistage Zeeman decelerator to generate slow beams ($v \simeq 100$ m/s) of translationally cold, spin-polarized metastable $a\,^3\Sigma_u^+$ He_2 molecules and perform a precision measurement of their spin-rotation fine structure. The spin polarization results from the elimination of the high-field-seeking $J = N$ spin-rotational component of each rotational level (rotational quantum number N) by the Zeeman deceleration process. By repopulating the $J = N$ component from the $J = N \pm 1$ low-field-seeking components using radio-frequency radiation, we measured the spin-rotation fine structure of 13 rovibrational levels with $v = 0$, 1 and $N = 1$–21. The low beam velocity and the resulting long interaction times with the radio-frequency radiation were exploited to determine the transition frequencies with a precision of 300 Hz.

DOI: 10.1103/PhysRevA.98.062518

I. INTRODUCTION

Samples of cold molecules [1–6] are ideally suited for precision spectroscopic measurements. They provide a collision-free environment and long interaction times with electromagnetic radiation fields and thus enable measurements at very high spectral resolution. These advantages are well illustrated by measurements of radio-frequency (rf) intervals in Stark-decelerated samples of the polar molecules $^{15}ND_3$ [7] and OH [8]. These measurements capitalize on the state selection, through the Stark-deceleration process, of molecules in low-electric-field-seeking states, i.e., the upper components of the tunneling doublets associated with the umbrella vibrational mode of $^{15}ND_3$ and the upper component of the Λ doublet of the lowest rovibrational levels of the $X^2\Pi$ ground state of OH. The same selection principle had already contributed to the success of the molecular-beam resonance method in precision spectroscopy [9].

Zeeman deceleration selects low-*magnetic*-field-seeking molecules, typically the upper components of spin-rotation multiplets. In this paper, we demonstrate the use of Zeeman deceleration in precision spectroscopic measurements of spin-rotation intervals in open-shell paramagnetic molecules. The method is applicable to different systems than Stark deceleration, such as nonpolar open-shell atoms and molecules. Specifically, we measured the spin-rotation fine-structure intervals of 13 rovibrational levels of the metastable $a\,^3\Sigma_u^+$ state of He_2, a four-electron molecule of fundamental interest, that has a radiative lifetime of about 18 s [10] and a magnetic moment of about two Bohr magneton, making it an ideal candidate for such studies.

The $a\,^3\Sigma_u^+$ state of He_2 (He_2^* from now on) is of particular interest in molecular physics because it is the ideal starting point for spectroscopic studies of triplet He_2, which represents the simplest example of an open-shell four-electron molecule. Measurements of the fine structure of He_2^* have therefore a long history. Lichten and co-workers [11–13] achieved a precision of about 10 kHz for the fine structure of the lowest three rotational levels (rotational quantum number $N = 1, 3, 5$) in the 1970s already, exploiting all the advantages of their molecular-beam magnetic-resonance apparatus. Their measurements were extended to the $N = 7, 9, 11, 25, 27, 29$ levels by Bjerre and co-workers in the 1990s [14–16], who achieved a similar precision using laser-rf double-resonance spectroscopy in fast neutral beams. These two remarkable sets of results have remained unsurpassed until today and have been included in all subsequent analyses of the spectrum of triplet He_2 (see, e.g., Refs. [17–19]). We report here on a measurement of the fine-structure intervals of He_2^* at a precision improved by more than an order of magnitude over these previous results.

The rotational structure (including spin-spin and spin-rotation fine structure) of vibrational states (v) of He_2^* is well described by an effective Hamiltonian appropriate for Hund's case (b) molecules in electronic states of Σ symmetry [20,21],

$$\hat{H} = B_v\vec{N}^2 - D_v\vec{N}^4 + H_v\vec{N}^6 + \tfrac{2}{3}\lambda_v\left(3S_z^2 - \vec{S}^2\right) + \gamma_v\vec{S}\cdot\vec{N}, \quad (1)$$

where $\vec{N}$ and $\vec{S}$ are the total angular momentum excluding spin and the electron spin, respectively, and B_v, D_v, and H_v are the usual rotational and centrifugal-distortion constants. The spin-spin and spin-rotation interactions are characterized by the coupling constants λ_v and γ_v, respectively. For high-resolution studies it is required to include centrifugal-distortion corrections for the spin-spin and spin-rotation parameters as well (see Refs. [18,22,23] for their definitions and corresponding matrix elements). The spin-spin and spin-rotation interactions split each rotational state with rotational quantum number N into three fine-structure components $J = N, N \pm 1$, as depicted for the $N = 1$ level in Fig. 1(b), which also shows how the energy levels are further split and shifted in the presence of a magnetic field.

*merkt@xuv.phys.chem.ethz.ch

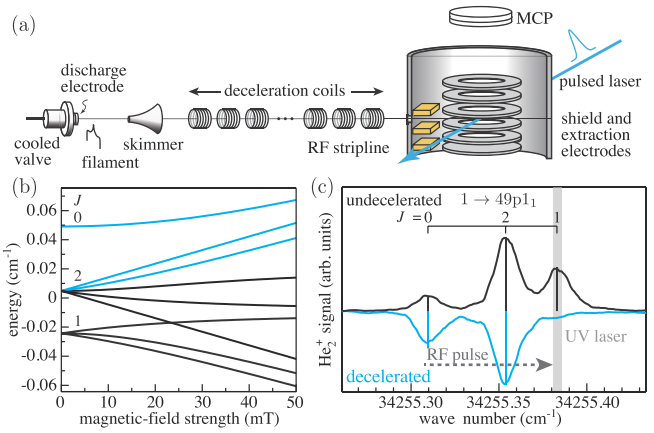

FIG. 1. (a) Schematic view of the experimental setup. (b) Zeeman effect of the $N = 1$, $J = 0$–2 levels of He_2^*. The low-field-seeking states are highlighted in blue. (c) Comparison of UV spectra of the $N = 1$, $J = 0 - 2 \rightarrow 49p1_1$ transition recorded with and without deceleration. The low-field-seeking components of the $J = N \pm 1 = 0, 2$ levels are decelerated, whereas Zeeman components of the $J = N = 1$ level are rejected during the deceleration process. To measure the spin-rotation transitions, an rf pulse, represented by the dashed arrow for the $N = 1$, $J = 0 \rightarrow J = 1$ rf transition, is used to repopulate the $J = N$ levels from the $J = N \pm 1$ levels.

II. EXPERIMENTAL PROCEDURE

The experimental setup and measurement procedure are schematically depicted in Fig. 1. A supersonic beam of He_2^* is produced in an electric discharge through an expansion of pure helium into vacuum [24]. The valve body is cooled to a temperature of 10 K with liquid helium, producing a molecular beam with a mean velocity of roughly 500 m/s [25]. After the molecules pass a skimmer, they can be decelerated to about 100 m/s using a 55-stage Zeeman decelerator. Because of the state selectivity of the deceleration process, only molecules residing in fine-structure levels of positive Zeeman shift [see the blue lines in Fig. 1(b)] are transmitted by the Zeeman decelerator [25]. Hence, the operation of the decelerator results in a spin-polarized beam by eliminating the $J = N$ fine-structure component of each rotational level [26,27]. The decelerated molecules traverse an rf stripline before being intersected at right angles by the doubled output of a pulse-amplified cw ring dye laser in the center of a cylindrically symmetric stack of electrodes. They are detected by UV-laser ionization or excitation to a high Rydberg state ($n \approx 50$) followed by pulsed-field ionization and extraction of the He_2^+ ions toward a microchannel-plate (MCP) detector. The rf stripline and the photoexcitation region are enclosed within a single-layer mumetal shield to reduce stray magnetic fields to ~10 mG.

Transitions between spin-rotational components of He_2^* are recorded using the rf-UV double-resonance excitation scheme illustrated in Fig. 1(c). First, a sample of undecelerated molecules is used to record a fine-structure resolved spectrum of transitions to high Rydberg levels. An example of such a spectrum, corresponding to a transition to a p Rydberg state with principal quantum number $n = 49$ and belonging to a series converging on the $N^+ = 1$ rotational level of the vibronic

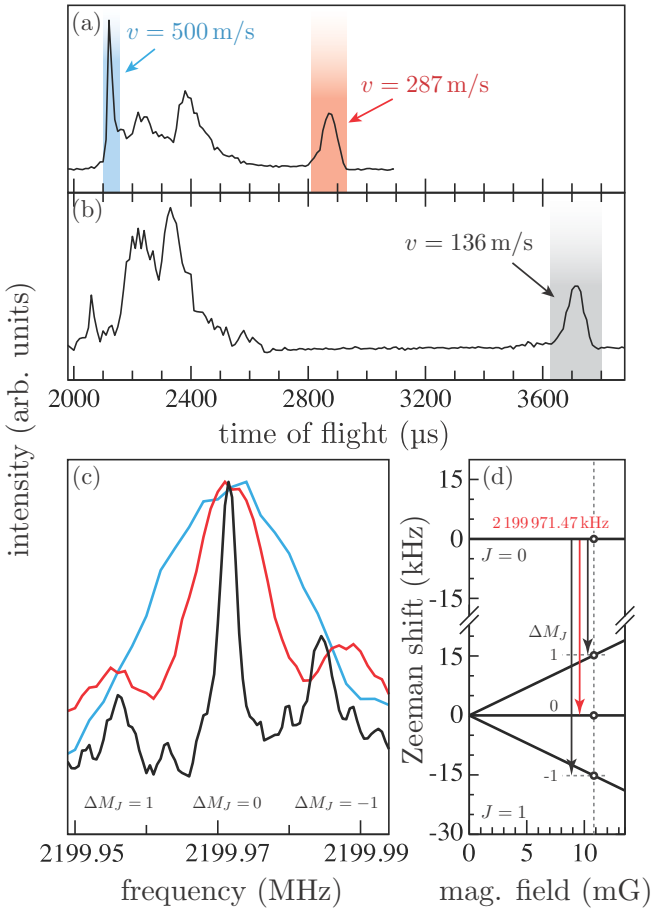

FIG. 2. (a, b) Time-of-flight distributions of the He_2^* beam after Zeeman deceleration. The deceleration was optimized to produce a packet of molecules with a velocity of 287 and 136 m/s in panels (a) and (b), respectively. (c) Recorded $J = 0 \rightarrow J = 1$ rf transition in molecular beams of 500 m/s (blue trace), 287 m/s (red trace), and 136 m/s (black trace). The FWHM of the transitions reduces from ~22 to 3 kHz because of the increased interaction time with the rf field. (d) Zeeman shift for the $J = 0$ and 1 levels for low magnetic field. The sidebands observed for the red and black trace in panel (c) indicate a stray magnetic field of ~11 mG.

ground state of He_2^+ ($49p1_1$ in the notation npN_N^+), is shown as the upper black trace in Fig. 1(c). The same spectral region is remeasured using a Zeeman-decelerated molecular beam. The corresponding spectrum, shown as the lower blue trace in Fig. 1(c), clearly demonstrates the elimination of the $J = N$ component. By keeping the UV-laser frequency fixed at the spectral positions of the rejected fine-structure component while scanning the frequency that is applied to the rf stripline, the signal from the $J = N$ component can be observed again if this level is repopulated by a pulse of rf radiation prior to the UV-laser excitation. The duration and timing of the rf pulse are optimized to maximize the interaction time with the molecules, while at the same time preventing the interaction region to extend beyond the mumetal shield.

III. RESULTS

Figures 2(a) and 2(b) show the intensity of the He_2^* beam after Zeeman deceleration as a function of the trigger delay

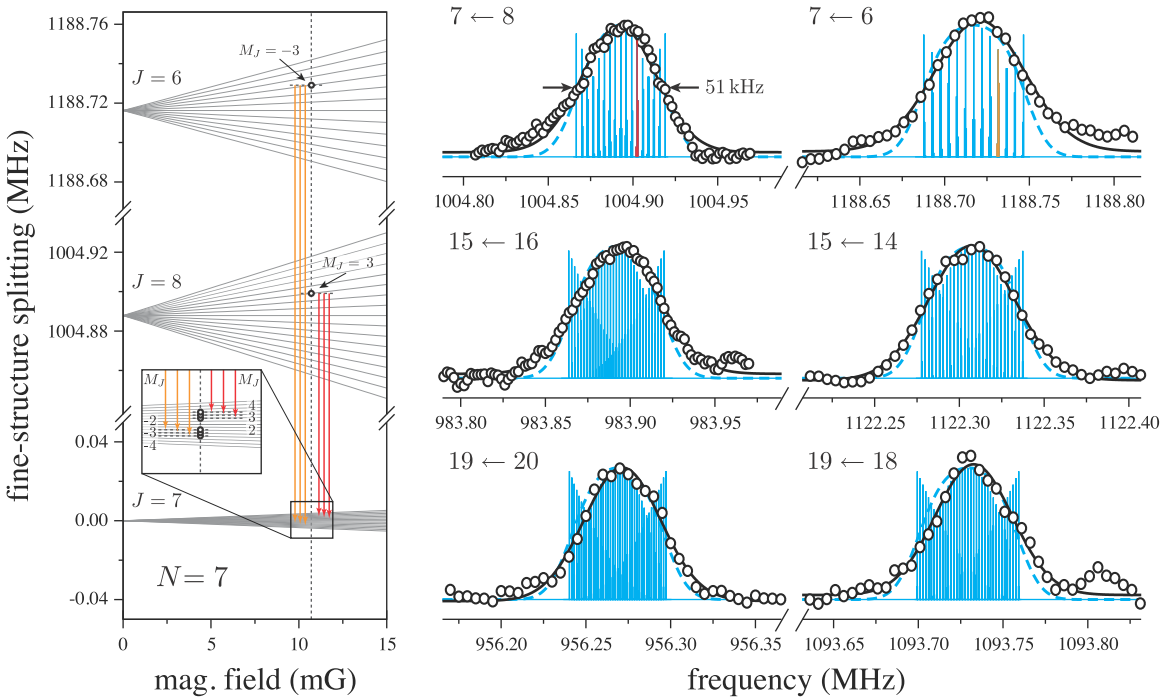

FIG. 3. Left panel: Zeeman structure of the spin-rotation components of the $N = 7$ rotational state for weak magnetic fields. The vertical orange and red arrows represent parallel and perpendicular transitions from the $M_J = -3$ and 3 magnetic sublevels of the $J = 6$ and 8 fine-structure components to magnetic sublevels of the $J = 7$ component in the presence of an 11-mG magnetic field, respectively. Right panels: Power-broadened rf spectra displaying the $J = N \pm 1 \leftarrow J = N$ $(v = 0)$ $(N = 7, 15, 19)$ transitions. The contribution of the transitions highlighted in red and orange on the left panel are shown in the same color in the corresponding spectrum.

between the valve opening and the ionization pulse, so that longer times correspond to lower velocities of the molecules. The trace in Fig. 2(b) was recorded by operating all coils of the decelerator and using a pulse sequence optimized for a final synchronous velocity of 136 m/s ($\phi_0 = 40°$, see Ref. [28] for details). The trace in Fig. 2(a) was measured using the same pulse sequence but operating only the first 42 coils of the decelerator, resulting in a final velocity of 287 m/s. The distributions presented in Figs. 2(a) and 2(b) clearly demonstrate that a significant part of the molecular beam is detected at delays around 2900 and 3700 μs, corresponding to velocities of 287 and 136 m/s, respectively. Operation of the Zeeman decelerator also results in partial focusing of molecules that do not belong to the phase-space volume accepted by the deceleration process. These molecules are detected at a delay of ~2100 μs, corresponding to a velocity of ~500 m/s.

Figure 2(c) shows rf spectra of the $N = 1$, $J = 0 \rightarrow J = 1$ magnetic-dipole fine-structure transition that was measured using He_2^* samples with mean velocities of 500 m/s (blue trace), 287 m/s (red trace), and 136 m/s (black trace) by selecting the appropriate delay [indicated by the arrows in Figs. 2(a) and 2(b)]. When recording these spectra, care was taken that the rf pulses did not broaden the transitions. To record the spectra corresponding to the higher velocities, the length of the rf pulses had to be slightly reduced to avoid contributions to the spectrum from molecules having moved to regions exposed to position-dependent stray magnetic fields. The FWHM of the transitions depicted in Fig. 2(c) decreases from ~22 to 3 kHz as the velocity of the sample is reduced, as expected from the longer interaction times with the rf field.

The black and red traces in Fig. 2(c) show two side bands separated by ~15 kHz from the stronger central line and that originate from the Zeeman splittings induced by a stray magnetic field of ~11 mG within the mumetal shield [see Fig. 2(d)]. In independent measurements, in which the rf pulse duration and intensity were varied, we ruled out that the side bands correspond to the side bands of the Rabi line shape. From the relative intensities of the parallel ($\Delta M = 0$) and the perpendicular ($\Delta M = \pm 1$) transitions, we can further estimate that the stray magnetic field makes an angle of ~15° with the magnetic field vector of the microwave radiation.

The same procedure can be used to measure the spin-rotation intervals of higher rotational levels. However, the number of Zeeman sublevels rapidly increases and the Zeeman shifts strongly depend on J, being much smaller for the $J = N$ component than for the $J = N \pm 1$ components, as illustrated in the left-hand panel of Fig. 3 for the $N = 7$ rotational level. Consequently, each spin-rotation transition is split into $2J + 1$ (with $J = N \pm 1$) closely spaced components that each may consist of up to three subcomponents. The spectral intensity is distributed over the resulting multitude of Zeeman components, which makes it difficult to detect the Zeeman substructure of the transitions at the 3-kHz resolution of our experiment. To observe the fine-structure transitions of higher rotational levels, we therefore power broaden the spectrum and observe the unresolved sum of all Zeeman components. Because the value of the stray magnetic field is known from the high-resolution measurement of the $N = 1$ fine structure, the broadened line profile can be accurately simulated and the field-free transition frequencies determined.

TABLE I. Frequencies (in MHz) of the transitions connecting the $J = N \pm 1$ and $J = N$ spin-rotation components of the rotational levels of the $a\,^3\Sigma_u^+$ ($v = 0, 1$) levels of He_2. The columns designated with Δ contain the residuals $\Delta = \nu_{obs.} - \nu_{calc.}$ after optimizing the spin-spin and spin-rotation constants including centrifugal corrections [see Eq. (1)].

		This work				Literature values	
v	N	$N-1 \rightarrow N$	$\Delta \times 10^4$	$N+1 \rightarrow N$	$\Delta \times 10^4$	$N-1 \rightarrow N$	$N+1 \rightarrow N$
0	1	2199.97147(29)	1.5	873.66959(35)	0.9	2199.968(10)[a]	873.668(7)[a]
	3	1323.907(4)	–53	964.999(4)	110	1323.911(6)[a]	964.992(6)[a]
	5	1227.023(3)	21	994.544(4)	17	1227.021(7)[b]	994.533(5)[b]
	7	1188.721(4)	37	1004.8919(24)	–10	1188.718(18)[c]	1004.886(21)[c]
	9	1166.450(3)	–3.6	1006.220(6)	160	1166.449(9)[c]	1006.217(18)[c]
	11	1150.075(4)	56	1002.160(5)	17	1150.073(12)[c]	1002.167(21)[c]
	13	1135.899(4)	–77	994.414(5)	–140		
	15	1122.3073(24)	–9.9	983.8936(24)	10		
	17	1108.4150(24)	7.1	971.0651(21)	2.2		
	19	1093.733(3)	23	956.272(3)	17		
	21	1077.959(7)	75	939.714(8)	–140		
	25					1042.360(3)[d]	901.965(8)[d]
	27					1022.314(3)[d]	880.956(3)[d]
	29					1000.634(6)[d]	858.607(5)[d]
1	1	2076.262(6)	–7.1	824.569(8)	23		
	3	1249.261(5)	7.7	910.622(5)	–7.3		
	25					973.401[d]	841.777[e]
	27					952.743[e]	820.326[e]

[a]From Ref. [11].
[b]From Ref. [13].
[c]From Ref. [14].
[d]From Ref. [15].
[e]N. Bjerre, private communication as reported in Ref. [18].

To this end, we calculate the Zeeman shifts as described in our previous work on the preparation of spin-polarized O_2 $X^3\Sigma_g^-$ molecules [29] and determine the relative intensities of the Zeeman components using standard angular-momentum algebra [30]. The right-hand side of Fig. 3 shows measurements of the spin-rotation transitions of the $N = 7$, 15, and 19 levels (open circles) along with simulated stick spectra of the expected magnetic substructure and a convolution with a 25-kHz Gaussian function (dashed blue line). The full black lines represent Gaussian profiles obtained in a fit to the experimental data. Because of the broadening resulting from the unresolved magnetic substructure, the fine-structure splittings of high rotational levels cannot be determined with the same accuracy as that of the $N = 1$ level, which has a fully resolved magnetic substructure [see Fig. 2(c)].

The frequencies of all observed transitions are listed in Table I, which includes values obtained for the rotational levels of the $v = 0$ state with $N \leqslant 21$ and the $v = 1$, $N = 1$ and 3 levels. These data represent the main result of the present investigation and enable a full characterization of the spin-rotation fine structure of the $a\,^3\Sigma_u^+$ state at low energies. They are in agreement with, but overall more accurate than, the results obtained for low ($N = 1 - 11$) and high ($N = 25 - 29$) rotational levels in earlier studies [11,13–15]. In the case of the $N = 1$ level, for which the full capability of our experiment could be exploited, the transition frequencies

TABLE II. Spin-spin and spin-rotation constants of the $a\,^3\Sigma_u^+$ ($v = 0, 1$) state of He_2 derived from the data presented in Table I. All values are given in MHz.

	This work		Literature values [18]	
	$v = 0$	$v = 1$	$v = 0$	$v = 1$
γ_v	− 2.42224(6)	− 2.28050(17)	− 2.4225(7)	− 2.254(3)
$\gamma_{Dv} \times 10^4$	6.856(10)	6.507(6)	6.844(21)	5.76(4)
$\gamma_{Hv} \times 10^8$	− 6.03(14)	− 5.34(6)	− 5.82(19)	
λ_v	− 1099.17016(12)	− 1037.3945(5)	− 1099.169(4)	− 1037.82(8)
λ_{Dv}	0.19748(5)	0.20143(8)	0.19752(11)	0.20251(11)
$\lambda_{Hv} \times 10^6$	− 4.68(24)	− 4.31(22)	− 4.78(28)	− 4.78[a]
$\lambda_{Lv} \times 10^9$	1.35(23)	1.67(16)	1.39(19)	1.39[a]

[a] Fixed to the value of the $v = 0$ level.

could be determined with a precision of about 300 Hz. The data in Table I were used to determine, in a weighted fit, the spin-spin and spin-rotation coupling constants γ_v and λ_v [see Eq. (1)], including the dominant centrifugal-distortion corrections [18,22,23]. The rotational and centrifugal-distortion constants associated with the end-over-end rotation of the molecule were kept fixed at the values reported by Focsa *et al.* [18].

The results of the fits are presented in Table II, and the residuals $\Delta = \nu_{\text{obs.}} - \nu_{\text{calc.}}$ are reported in the fourth and sixth columns of Table I. Compared to the earlier analysis by Focsa *et al.* [18], the leading terms γ_v and λ_v could be improved by more than an order of magnitude, and the coupling constants for $v = 1$ could be determined without having to fix the centrifugal-distortion fine-structure constants to the value of the $v = 0$ level.

IV. CONCLUSIONS

The improved characterization of the fine structure of the rotational levels of metastable He_2 reported in this paper results not only from the observation of the fine structure of levels that could not be measured so far, but mostly also from the long observation time, of the order of a millisecond, made possible by the Zeeman deceleration. This advantage was fully exploited in the measurement of the $v = 0$, $N = 1$ levels, as discussed above. Such long observation times would otherwise only be possible in a Ramsey-type experiment including two separate coherent driving fields. However, given the low He_2^* molecular density, their sensitivity to inhomogeneous magnetic fields, and the fact that the observed lines at high N values consist of multiple unresolved magnetic components, it is questionable whether Ramsey fringes could be observed at all in this system.

The results reported in this article represents one of the very rare examples of the use of cold-molecule-preparation techniques to significantly improve a previous spectroscopic result. The method of measuring the spin-rotation fine structure, on which this investigation relied, is applicable to a broad range of open-shell molecules, including polyatomic radicals to which multistage Zeeman deceleration could be successfully applied recently [31,32].

ACKNOWLEDGMENTS

This work was supported by the Swiss National Science Foundation (Grant No. 200020-172820), the Swiss National Competence Center for Research (NCCR QSIT), and the European Research Council (ERC) under the European Union's Horizon 2020 Research and Innovation Program (Advanced Grant No. 743121).

[1] A. Fioretti, D. Comparat, A. Crubellier, O. Dulieu, F. Masnou-Seeuws, and P. Pillet, Phys. Rev. Lett. **80**, 4402 (1998).
[2] H. L. Bethlem, G. Berden, and G. Meijer, Phys. Rev. Lett. **83**, 1558 (1999).
[3] S. Y. T. van de Meerakker, H. L. Bethlem, N. Vanhaecke, and G. Meijer, Chem. Rev. **112**, 4828 (2012).
[4] E. Narevicius and M. G. Raizen, Chem. Rev. **112**, 4879 (2012).
[5] S. D. Hogan, M. Motsch, and F. Merkt, Phys. Chem. Chem. Phys. **13**, 18705 (2011).
[6] E. S. Shuman, J. F. Barry, and D. DeMille, Nature (London) **467**, 820 (2010).
[7] J. van Veldhoven, J. Küpper, H. L. Bethlem, B. Sartakov, A. J. A. van Roij, and G. Meijer, Eur. Phys. J. D **31**, 337 (2004).
[8] E. R. Hudson, H. J. Lewandowski, B. C. Sawyer, and J. Ye, Phys. Rev. Lett. **96**, 143004 (2006).
[9] N. F. Ramsey, *Molecular Beams* (Clarendon Press, Oxford, 1956).
[10] C. F. Chabalowski, J. O. Jensen, D. R. Yarkony, and B. H. Lengsfield III, J. Chem. Phys. **90**, 2504 (1989).
[11] W. Lichten, M. V. McCusker, and T. L. Vierima, J. Chem. Phys. **61**, 2200 (1974).
[12] T. L. Vierima, J. Chem. Phys. **62**, 2925 (1975).
[13] W. Lichten and T. Wik, J. Chem. Phys. **69**, 98 (1978).
[14] M. Kristensen and N. Bjerre, J. Chem. Phys. **93**, 983 (1990).
[15] I. Hazell, A. Norregaard, and N. Bjerre, J. Mol. Spectrosc. **172**, 135 (1995).
[16] N. Bjerre, A. O. Mitrushenkov, P. Palmieri, and P. Rosmus, Theor. Chem. Acc. **100**, 51 (1998).
[17] S. A. Rogers, C. R. Brazier, P. F. Bernath, and J. W. Brault, Mol. Phys. **63**, 901 (1988).
[18] C. Focsa, P. F. Bernath, and R. Colin, J. Mol. Spectrosc. **191**, 209 (1998).
[19] C. Li, L. Deng, J. Zhang, X. Yang, Y. Chen, and L. Ma, J. Mol. Spectrosc. **260**, 85 (2010).
[20] J. M. Brown and A. Carrington, *Rotational Spectroscopy of Diatomic Molecules* (Cambridge University Press, Cambridge, UK, 2003).
[21] H. Lefebvre-Brion and R. W. Field, *The Spectra and Dynamics of Diatomic Molecules* (Elsevier, Amsterdam, 2004).
[22] J. M. Brown, E. A. Colbourn, J. K. G. Watson, and F. D. Wayne, J. Mol. Spectrosc. **74**, 294 (1979).
[23] C. R. Brazier, R. S. Ram, and P. F. Bernath, J. Mol. Spectrosc. **120**, 381 (1986).
[24] M. Raunhardt, M. Schäfer, N. Vanhaecke, and F. Merkt, J. Chem. Phys. **128**, 164310 (2008).
[25] M. Motsch, P. Jansen, J. A. Agner, H. Schmutz, and F. Merkt, Phys. Rev. A **89**, 043420 (2014).
[26] P. Jansen, L. Semeria, L. Esteban Hofer, S. Scheidegger, J. A. Agner, H. Schmutz, and F. Merkt, Phys. Rev. Lett. **115**, 133202 (2015).
[27] P. Jansen, L. Semeria, and F. Merkt, J. Mol. Spectrosc. **322**, 9 (2016).
[28] A. W. Wiederkehr, S. D. Hogan, and F. Merkt, Phys. Rev. A **82**, 043428 (2010).
[29] A. W. Wiederkehr, H. Schmutz, M. Motsch, and F. Merkt, Mol. Phys. **110**, 1807 (2012).
[30] R. N. Zare, *Angular Momentum: Understanding Spatial Aspects in Chemistry and Physics* (John Wiley & Sons, New York, 1988).
[31] T. Momose, Y. Liu, S. Zhou, P. Djuricanin, and D. Carty, Phys. Chem. Chem. Phys. **15**, 1772 (2013).
[32] Y. Liu, M. Vashishta, P. Djuricanin, S. Zhou, W. Zhong, T. Mittertreiner, D. Carty, and T. Momose, Phys. Rev. Lett. **118**, 093201 (2017).